Recombination activity associated with thermal donor generation in monocrystalline silicon and effect on the conversion efficiency of heterojunction solar cells

M. Tomassini,[1,a)] J. Veirman,[1,a)] R. Varache,[1] E. Letty,[1] S. Dubois,[1] Y. Hu,[2] and Ø. Nielsen[2]
[1]*CEA, LITEN, Department of Solar Technologies–National Institute of Solar Energy, F-73375 Le Bourget du Lac, France*
[2]*NorSun AS, Karenslyst Allé 9C, 0278 Oslo, Norway*

(Received 12 November 2015; accepted 5 February 2016; published online 29 February 2016)

The recombination properties of the carrier lifetime-limiting center formed during the generation of oxygen-related thermal donors (so called "old" thermal donors) in n-type Czochralski silicon were determined over a wide range of thermal donors' concentrations. The procedure involved (1) determining the various energy levels associated with dopants with the help of temperature Hall effect measurements, (2) clarifying which energy level limits the carrier lifetime by temperature lifetime spectroscopy, and (3) determining the recombination parameters of the involved defect from room-temperature carrier lifetime curves. Our results support the fact that a deep energy level in the range of 0.2–0.3 eV below the conduction band limits the carrier lifetime. The second family of thermal donors, featuring bistable properties, was tentatively identified as the corresponding defect. From the obtained experimental data, the influence of the defect on the amorphous/crystalline silicon heterojunction solar cell conversion efficiency was simulated. It is observed that for extended donor generation, the carrier lifetime is reduced by orders-of-magnitude, leading to unacceptable losses in photovoltaic conversion efficiency. A key result is that even for samples with thermal donor concentrations of $10^{15}\,cm^{-3}$—often met in seed portions of commercial ingots—simulations reveal efficiency losses greater than 1% absolute for state-of-the-art cells, in agreement with recent experimental studies from our group. This result indicates to crystal growers the importance to mitigate the formation of thermal donors or to develop cost-effective processes to suppress them at the ingot/wafer scale. This is even more critical as ingot cool-down is likely to be slower for future larger ingots, thus promoting the formation of thermal donors. © *2016 AIP Publishing LLC*.
[http://dx.doi.org/10.1063/1.4942212]

I. INTRODUCTION

It has been long known that during annealing in the 350–500 °C temperature (T) range, thermal donors (TD) are generated in Czochralski (Cz) silicon (Si) in the range of 10^{13}–$10^{15}\,cm^{-3}$ (Refs. 1 and 2) and can be annihilated above 600 °C.[3] To distinguish them from the later discovered New and Shallow thermal donors,[2] these donors are generally referred to as "old" thermal donors, and will be labeled TD in this work. TD are believed to be interstitial oxygen (O_i) aggregates.[4] They are preferentially formed in the ingot half crystallized first, as it generally contains more O_i (TD generation is very highly dependent on O_i concentration[5] ($[O_i]$)) and spends more time in the 350–500 °C range due to slower cooling rates. Using Hall effect and infrared analyses, up to 16 families of TD were resolved,[6–8] forming sequentially in the course of annealing (TD1, TD2…TD16). They are helium-like centers, i.e., they introduce two energy levels (E), located for all families in the vicinity of $E_1 = 0.05$ eV (E(0/+)) and $E_2 = 0.15$ eV (E(+/++)) below the bottom of the conduction band (E_c).[9,10] Considering these two relatively shallow levels, TD are doubly ionized at room T for standard doping levels used for photovoltaic applications (i.e., they provide each two free electrons). Due to their double-donor character, they induce a downward resistivity (ρ) shift in phosphorus (P)-doped ingots compared to what is expected from segregation laws of P, as they add up to the intentional doping. The larger $[O_i]$ and the longer the dwell time in the 350–500 °C range, the larger the ρ shift for a given intentional doping. Note that the resulting shift is generally higher at the ingot center (wafer center) due to larger $[O_i]$. In addition to a longitudinal ρ shift, TD thus also introduce a radial ρ shift if no particular control of the radial $[O_i]$ distribution is implemented.[11]

More detailed analyses based on Hall effect measurements,[12,13] infrared spectroscopy,[14,15] and Deep Level Transient Spectroscopy (DLTS)[16] evidenced that the two defect families formed first in the course of annealing (TD1 and TD2) feature bistable properties. In other words, TD1 and TD2 can exist in two different structural configurations: the historically studied configuration "H" associated with two levels E_1 and E_2, and a second one labeled "X." TD1 and TD2 in configuration X also introduce two E, with the particularity that—unlike TD in configuration H—the second electron is bound more strongly than the first. Such centers are called Anderson systems with negative correlation energy (or "negative-U" systems).[17,18] They effectively act as a unique level E(0/++), since for such centers the charge

[a)]M. Tomassini and J. Veirman contributed equally to this work.

state + is unlikely. The corresponding E(0/++) were measured by Hall effect in 375 °C annealed samples to be located at around E_c-0.32 eV and E_c-0.23 eV, respectively, for TD1 and TD2.[14] They were later observed at similar positions in as-grown samples[19] as well as after 430 °C anneals.[10,20] Note that, as will be discussed below, only E_1 and E_2 associated with configuration H are empty (i.e., ionized) at room T for standard ρ (Fermi level energy (E_F) located at about E_c-0.2 eV), while the X configuration is statistically neutral. Therefore, the defect concentrations reported in the literature using ρ measurements at room T are those of TD in the H configuration only. To facilitate comparison with previous works, the reader should bear in mind throughout this paper that the concentration term "[TD]" will implicitly refer to that concentration of defects in configuration H, while the notation "TD" still refers to the defect regardless of its configuration.

As TD are generally suppressed during the high T steps of homojunction cell processes or microelectronic devices, their influence on the bulk carrier lifetime (τ_{bulk}) has been historically poorly investigated. Nevertheless, this topic has recently gained attention[21–26] with the developments of high efficiency low T solar cell processes based on an amorphous Si/crystalline Si heterojunction (HET), associated with very high efficiencies. As the maximum T in the course of such processes remains usually below 300 °C, TD are retained in the bulk of the cell even after module encapsulation. It is therefore critical to assess their effect on HET cells properties. In this regard, it is well-known that TD can strongly reduce the majority and minority carrier mobilities (μ) for concentrations above $10^{15}\,cm^{-3}$.[27,28] Indeed their double donor character confers them a scattering power which is fourfold that of a singly ionized impurity such as P or boron. However, for [TD] below $1–1.5 \times 10^{15}\,cm^{-3}$ as observed in commercial wafers, the μ are only slightly lower than in a material with a P doping yielding the same ρ value (maximum 10%). The present paper will therefore not address these effects.

On the other hand, the multi-milliseconds τ_{bulk} requirements of HET cell architectures[29] make the study of TD recombination properties highly relevant. This study is also motivated by the fact that favored TD generation will occur as the length of Cz ingots—and therefore their thermal mass—will increase. Recently, Hu *et al.* observed a significant effective lifetime (τ_{eff}) drop from around 2 ms to 600 μs when going from $[TD] < 10^{14}\,cm^{-3}$ to $10^{15}\,cm^{-3}$.[21] This was in parallel confirmed by Jay *et al.*, who measured a τ_{eff} of around 150 μs for a $[TD] = 2 \times 10^{15}\,cm^{-3}$.[23] However, the nature of the recombination center(s) at the origin of these reduced τ_{eff} is still unclear and so are the associated recombination properties. Since TD are both dopants and potential recombination-active defects, it is not clear whether the observed reductions originate from a mere doping effect, or from the addition of recombination centers in the material. Note that some authors did not evidence such strong τ_{eff} reduction after TD generation.[19,25] However, essential details were either lacking to explain these results (TD generation conditions, procedure to determine [TD]),[19] or the surface passivation quality was not high enough to detect τ_{bulk} changes upon TD generation.[25]

In this context, the aim of the present paper is twofold. The first goal is to identify and characterize the τ_{bulk}-limiting defect(s) in TD containing Si, using temperature and injection-level dependent lifetime spectroscopy (TIDLS) measurements, in conjunction with temperature Hall effect measurements. The second goal is to investigate the effect of TD on the HET solar cell efficiency (η), via simulations based on the obtained experimental data.

II. MATERIALS SELECTION AND EXPERIMENTAL DETAILS

A. Studied wafers

The studied wafers were sampled from the top block of an 8 in. commercial n-type P-doped Cz ingot. Six adjacent 180 μm thick wafers were sampled, whose compositions can be considered virtually identical. The wafers were carbon-lean (<0.1 ppma) and dislocation-free. All wafers were etched using an alkaline KOH solution to remove the saw-damaged layer. Particularly, this step prevents in-diffusion from impurities in the bulk during subsequent thermal treatments. After this etching step, a first wafer (B) was kept as-etched, and thus contained its own TD concentration formed during cool-down ($[TD_{ini}]$). A second wafer (A) was used to measure the P concentration ([P]). This was achieved through a 4 point-probe ρ measurement after a TD anneal (TDA) at 800 °C for some seconds in a belt furnace, leaving the wafer virtually free of TD. [P] was found equal to $4.2 \times 10^{14}\,cm^{-3}$ using standard μ models[30] for the ρ-to-doping conversion. Note that all reported ρ measurements were performed using the 4 point-probe technique at room T (294 K).

The remaining wafers (C, D, E, and F), which also contained the same amount of TD_{ini} and P, were subsequently subjected to 450 °C heat treatments in order to generate additional TD (TD_{450}). The anneals were performed in a clean furnace under nitrogen flow to limit unintentional contamination. Following each annealing sequence, the samples were brought to room T in a few minutes, so that the formation of low T defects is unlikely to occur in quantity that would impact our findings (mostly vacancy-related defects[31,32]). The 450 °C anneal durations were chosen so as to generate various desired [TD], following the method given in Ref. 27. The latter method involves beforehand the determination of $[O_i]$ on an as-cut sister wafer using the Oxymap method first introduced in Ref. 33 and updated in Ref. 34. $[O_i]$ was found to be $7.4 \times 10^{17}\,cm^{-3}$. Then, the expected [TD] evolution at 450 °C was calibrated using the latter $[O_i]$, and the wafers were annealed in such a way as to generate the desired [TD]. The anneal durations varied from 0 to 206 h. Then, the total $[TD] = [TD_{ini}] + [TD_{450}]$ for 450 °C annealed wafers were confirmed from temperature Hall effect measurements (see Sec. III A). The range of [TD] generated varies from virtually 0 to $6.9 \times 10^{15}\,cm^{-3}$ and therefore allows the TD effect on τ_{bulk} and on HET cells performances to be investigated in-depth. The composition of all wafers is given in Table I.

TABLE I. Description of samples.

Sample	[P] (cm^{-3})	ρ (Ω cm)	[TD_{ini}] (cm^{-3})	[TD] (cm^{-3})	450 °C anneal time (h)
A	4.2×10^{14}	9.89	Traces	Traces	TDA
B	4.2×10^{14}	4.58	1.9×10^{14}	1.9×10^{14}	0
C	4.2×10^{14}	1.65	1.9×10^{14}	1.1×10^{15}	15
D	4.2×10^{14}	0.64	1.9×10^{14}	3.7×10^{15}	82
E	4.2×10^{14}	0.54	1.9×10^{14}	4.5×10^{15}	130
F	4.2×10^{14}	0.45	1.9×10^{14}	6.9×10^{15}	206
G	7.0×10^{14}	1.38	1.4×10^{15}	1.4×10^{15}	0

For Hall effect measurements, an extra wafer (G) taken from the top of another commercial ingot was included in the study. Wafer G had a high [O_i] of $1.0(5) \times 10^{18}\,cm^{-3}$ and a resulting high [TD_{ini}] of $1.4 \times 10^{15}\,cm^{-3}$, considered as an upper value found in nowadays commercial wafers. Wafer G was not 450 °C annealed. Note that wafer G features very similar [TD] to wafer C. Nevertheless, TD were formed at 450 °C in wafer C whereas they were unintentionally formed between around 350 and 500 °C during ingot cool down in wafer G. Therefore, by comparison of the E positions in the band-gap observed in both samples, the influence of the annealing T on the E positions will be studied.

All wafers were cut into two samples prepared from the wafer center. The first sample was dedicated to Hall effect measurements and was $2 \times 2\,cm^2$ large. The other one, in the shape of a $5.2 \times 15.6\,cm^2$ strip, was taken right next to the Hall sample and was dedicated to τ measurements. This cutting scheme ensured that Hall effect and τ_{eff} measurements could be performed as close as possible to the wafer center, so that lateral variations in [TD] were minimized.[35] The overall procedure used in this work is summarized in Figure 1.

B. Energy levels and concentrations of thermal donors in "H" configuration

In order to investigate the composition of the investigated samples, temperature Hall effect measurements were conducted from 77 K to 350 K using an Ecopia HMS 5000 system. The electrical contacts were performed in the corners of all samples using a liquid InGa eutectic embedded in the Si matrix using a diamond point. The samples were first quenched to 77 K by dipping them into liquid nitrogen. Then, the measurement sequence was immediately started (T step of 5 K). Both cooling and heating were performed in the dark. Such a procedure allowed to limit possible interchanges in the relative proportions of TD configurations X and H.[13,16] For each T, the raw Hall concentrations (n_H) were corrected to yield the "true" experimental carrier concentrations (n_0). To this end, n_H measured at a given T was multiplied by the corresponding value of the Hall factor (r_H) at this T, as given in Ref. 36. As r_H values below 100 K are not provided in the latter reference, it was assumed that $r_H(T) = r_H(100\,K)$ for $T < 100$ K. The $n_0 = f(T)$ experimental curves were then fitted using the following expression which arises from the charge neutrality equation applied to n-type Si containing TD, in combination with the use of Fermi-Dirac statistics to describe the occupation probabilities of dopant levels:[37]

$$n_0 = N_C \times \exp\left(\frac{E_F - E_C}{k_B T}\right) = \frac{[P]}{1 + g_P \times \exp\left(\frac{E_F - E_P}{k_B T}\right)} + \frac{\beta \times (1 + 2\alpha)}{1 + \beta + \alpha\beta} \times [TD], \quad (1)$$

where N_c, E_c, E_F, and k_B have their usual meanings. E_P is the P energy level (E_c-0.0455 eV (Ref. 38)), and the degeneracy factor (g) of E_P is called g_P and is equal to 2 in the notation used.

The terms α and β are, respectively, expressed as

$$\alpha = \frac{1}{g_2} \times \exp\left(\frac{E_2 - E_F}{k_B T}\right), \quad (2)$$

$$\beta = \frac{1}{g_1} \times \exp\left(\frac{E_1 - E_F}{k_B T}\right), \quad (3)$$

where g_1 and g_2 are, respectively, the degeneracy factors of E_1 and E_2, with $g_1 = 0.5$ and $g_2 = 2$ (Refs. 37 and 39) in the chosen notation. For each T and for a given tentative set of values of [TD], E_1 and E_2, Eq. (1) was solved with respect to E_F. Using the computed E_F, n_0 was subsequently calculated for each T. The set of input values was varied until the

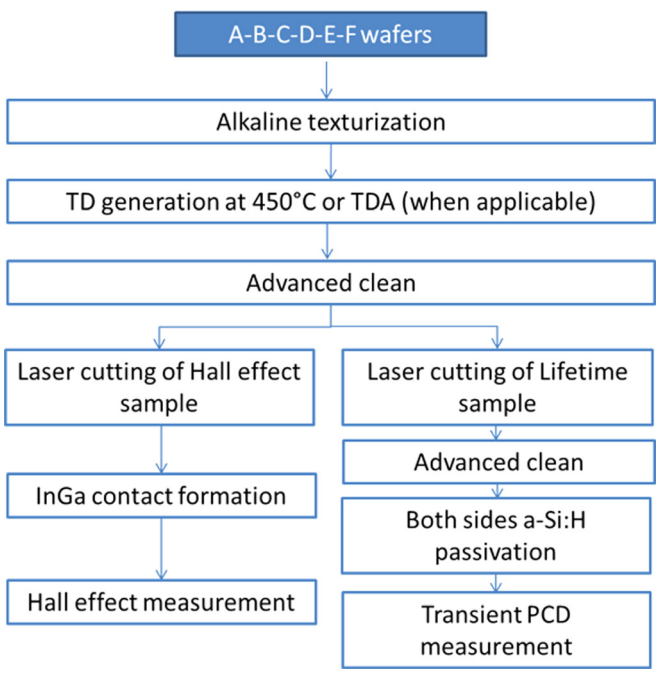

FIG. 1. Procedure used in this work.

optimal fit to the experimental $n_0 = f(T)$ curve was achieved. For each sample, this procedure allowed the determination of unique values for E_1, E_2, and [TD].

This technique is very powerful when applied to samples with known dopants (intentional or not), as the dopant species assumed to be present in the sample determine the form of Eq. (1). In more complex cases, with multiple unknown doping centers/center configurations, it can be useful to use alternative techniques such as Hall effect spectroscopy, as introduced by Hoffmann.[40]

C. Hall effect spectroscopy and dopant energy levels

Hall effect spectroscopy was used to determine the different E introduced by dopants in the studied samples. This procedure relies on the fact that a majority impurity (i.e., having E in the upper half of the bandgap in n-type Si) is progressively ionized upon T increase. This occurs in n-type Si whenever E_F crosses downwards an energy level introduced by a given defect, in the course of heating. In doing so, the defect E is progressively emptied, with a maximum "emptying rate" $-dn_0/dE_F$ happening when E_F coincides with E. The plot of $-dn_0/dE_F$ versus E_C-E_F thus shows maxima, whose abscissa provide the positions of the different E. In case g is different from unity, the maxima are slightly shifted by $kT_{peak} \times \ln(g)$ on the energy scale,[40] where T_{peak} is the value of T at which the peak is observed. This correction was made when necessary.

D. Carrier lifetime measurements and identification of the carrier lifetime-limiting energy level

It is postulated that recombination occurs only on one E in the studied samples. Indeed comparable recombination activities through multiple E is seldom, but will nevertheless be discussed in the light of the obtained results in Sec. III C. In an attempt to clarify its nature, Temperature Dependent Lifetime Spectroscopy (TDLS) was performed on samples dedicated to τ_{eff} measurements using a temperature WCT120 from Sinton Instruments. Prior to τ_{eff} measurements, the lifetime samples were cleaned using an advanced ozone-based procedure followed by a deoxidization with an hydrofluoric acid solution. Finally, hydrogenated amorphous Si (a-Si:H) layers were deposited by PECVD on both sides to passivate the surfaces. This step was performed at low T (~200 °C) and should thus have a limited effect on the defects present in the samples. In order to avoid any unexpected transient in the passivation properties of the a-Si:H layers, the lifetime samples were annealed at 200 °C under ambient light for around seven hours prior to the measurements. A slight increase in around 10% in the room T τ_{eff} was observed on all samples after this stabilization step. This can arise from a passivation improvement and/or annealing of vacancy-related defects as recently observed in Refs. 31 and 32.

At low injection level ($\Delta n \ll n_0$), the variations of the Shockley-Read-Hall (SRH) lifetime (τ_{SRH}) with T obey the following law, ΔE_t being the energy difference between the E position of the lifetime-limiting defect (E_t) and the extremum of the closest band (positive value)[41]

$$\tau_{SRH} = T^{\alpha+1} \times \exp(-\Delta E_t / k_B T), \tag{4}$$

where α is the T coefficient of the capture cross section for minority holes (σ_p), assumed to follow a power law $\sigma_p = \sigma_0 \times T^{-\alpha}$. Note that the T range used varied from 21 to 185 °C on our TDLS setup.

In the inductively coupled photoconductance decay (IC-PCD) technique associated with the WCT120, the ρ value provided by the user is transformed into a doping concentration, which is then used to estimate the μ sum needed to calculate Δn.[42] In our case, the calculation yields slightly incorrect μ sum values, since it tacitly implies that the samples be doped with singly ionized dopants, which is not the case here. To circumvent this, the μ sum was calculated for each sample using traditional mobility models[30] taking into account the four-fold enhanced scattering power of TD compared to P atoms. Then, the fictive ρ value giving the calculated μ sum was chosen as input value in the spreadsheet. It was found that the fictive ρ values thus determined lead to a maximum shift in the τ_{eff} curve of 2.5% upwards. This effect was only taken into account for the room T measurements, but could as well be simply ignored.

At the highest measured Δn (several $10^{16}\,cm^{-3}$), the quasi Fermi level for electrons is significantly higher than E_F in the dark. As a consequence, a significant fraction of TD may switch from a double to a single charge state when Δn increases. As a result, this is likely to invalidate our calculations made to determine the fictive ρ to be used in the dark as an input parameter. This effect was however computed to lead to a maximum downward τ_{eff} shift of 3.5% at high Δn and was therefore neglected.

In order to determine the recombination parameters of the lifetime-limiting defect, the resulting τ_{eff} curves were then adjusted using the following expression:

$$\frac{1}{\tau_{eff}} = \frac{1}{\tau_{SRH}} + \frac{1}{\tau_{int}} + \frac{1}{\tau_{surf}}, \tag{5}$$

where τ_{int} is the intrinsic limit due to Auger and radiative recombination channels, as computed from the model by Richter *et al.*[43] τ_{surf} is the lifetime limited by surface recombination and is given by $w/(2S_{eff})$, where w is the wafer thickness and S_{eff} is the effective surface recombination velocity. S_{eff} and its variation with Δn were estimated from τ_{eff} measurements on high-quality passivated samples following the method in Ref. 44. S_{eff} was found to vary in the range of 1–2 cm s^{-1}. Although τ_{surf} may slightly vary with ρ, an empirical parameterization of the τ_{surf} versus Δn curve obtained with $\rho = 3\ \Omega$ cm was used for the fitting procedure for all wafers, whatever their ρ.

Eventually, τ_{SRH} was adjusted to fit the experimental curves by changes of the recombination active defect level E_t, its concentration (N_t), and its capture cross sections for holes and electrons (σ_p and σ_n) using the simplified SRH expression detailed in Refs. 45 and 46.

E. Solar cells simulation details

The package Atlas from Silvaco was used to study the influence of donor generation on the HET cell performances.

The basic structure includes a crystalline Si (c-Si) wafer passivated with a-Si:H on both sides, and Indium Tin Oxide (ITO) transparent conductive front and back layers. More details regarding the simulated structures, modeling standard HET cells, can be found in Ref. 47. It is worth noticing that front and back emitter structures are simulated to make the results as general as possible. All materials, c-Si, a-Si:H, and ITO are modeled as bulk semiconductors. Both front and rear emitter cells were simulated in 2 dimensions to include lateral transport towards front localized metallic contacts. For each structure, a commercial cell (around 21%) was simulated along with an advanced cell (23%) under standard test conditions (25 °C, 1000 W m^{-2}, AM1.5 G spectrum). For the commercial cell, interface defect density and series resistance were set in order to match the cell performances achieved on the HET pilot line at CEA-INES; on the contrary, the advanced cell has a low series resistance (and thus higher FF, achievable, for example, with new TCOs or metallization schemes) and a low interface defect density.

Regarding material parameterization, the doping data as well as the SRH recombination parameters determined experimentally were used as inputs in the model. The doping concentration entered into Silvaco Atlas corresponds to $n_0 = [P] + 2 \times [TD]$, since TD provide each two free electrons at room T. Note that the spatial distribution of TD across the wafers (highly inhomogeneous in practice) was considered constant, in order to simplify the interpretation of the simulation results. It is expected that simulations run with actual TD spatial distributions would somehow show lower FF and hence efficiencies.[11] For SRH statistics, a single donor-like defect level was inserted in the upper part of the band gap, with E_t, σ_p, σ_n, and N_t as determined experimentally. Complementary details about the simulation (metallic contacts, a-Si:H properties, and TCO properties) can be found in Ref. 47.

III. RESULTS

A. Energy levels and concentrations of the doping species in presence

The $n_0 = f(T)$ experimental curves are shown in Figure 2, along with the associated fits using Eq. (1). In Eq. (1), [P] is known from ρ after TD killing. The progressive release of electrons to the conduction band as T increases reveals the influence of 3 distinct E for all samples, except for sample A (TDA sample). Sample A shows only the release of electrons from the P atoms, suggesting that the three evidenced E were efficiently suppressed during TDA. Note that those step-releases of electrons were also observed as kinks in $\rho = f(T)$ measurements using the van der Pauw technique (not shown here). We are therefore confident that the observed E are physical and are not measurement artifacts.

[TD], E_1, and E_2 were obtained from the best fits shown in Figure 2 (in the sense of least mean squares) and are given in Table II. The values found for E_1 and E_2 match very well previously reported values for TD, such as 0.075 and 0.170 eV below E_c in Ref. 9 or 0.055 and 0.140 eV in Ref. 10. This confirms that E_1 and E_2 correspond, respectively, to the shallow E(0/+) and the deeper E(+/++) levels

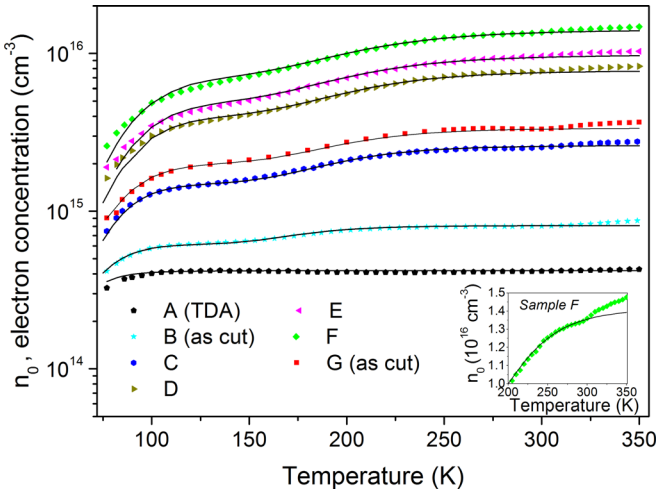

FIG. 2. Experimental $n_0 = f(T)$ data (symbols) and associated fits (solid lines) using Eq. (1). The approximate positions where the energy levels (E) are ionizing upon T increase are indicated by arrows. The inset is a zoom on the high T region for sample F and shows ionization of E_3.

introduced by the H configuration of TD. In relation to the form of Eq. (1), a unique concentration ([TD] in fact) allowed both E_1 and E_2 progressive ionization to be satisfactorily adjusted; this validates the expected result that both E_1 and E_2 are associated with TD in configuration H. Conversely, the level E_3 is shown not to be related directly to configuration H of TD, as the concentration of free electrons released by this level in the range of 300–350 K is much lower than [TD].

At this point, it is worth noticing that, on a more practical aspect, the release of additional electrons by E_3 in the 300–350 K range (in the range of 10^{14}–10^{15} cm^{-3}) induces a change in n_0 from room T to higher operating T (solar modules in outdoor conditions, for instance). Under standard outdoor illumination, however, this additional electron release is small compared to the supply of excess carriers from light in high efficiency HET cells (usually $>10^{15}$ cm^{-3} under a standard 1000 W m^{-2} illumination at 25 °C). It should thus not be noticeable.

Equation (1) used to fit the data does not take into consideration the electron release from E_3. Therefore, only [TD], E_1 and E_2 were determined. Hall effect spectrometry was then used to determine the missing positions of E_3 in the

TABLE II. [TD], E_1, E_2, E_3, and [X] values for the studied samples. The uncertainties for [TD], E_1 and E_2 are estimated from the loss in fitting quality by changing the input parameters. They are ±5% on [TD] and ±5% on the positions of the different E. The values given for [X] underestimate at most by 20% the actual values (see text).

Sample	[TD] (cm^{-3})	E_c-E_1 (eV)	E_c-E_2 (eV)	E_c-E_3 (eV)	[X] (cm^{-3})
A	Traces	…	…	…	Undetected
B	1.9×10^{14}	0.068	0.139	0.301	5.6×10^{13}
C	1.1×10^{15}	0.065	0.140	0.242	1.9×10^{14}
D	3.7×10^{15}	0.064	0.130	0.211	4.9×10^{14}
E	4.5×10^{15}	0.064	0.126	0.200	6.3×10^{14}
F	6.9×10^{15}	0.061	0.122	0.199	9.1×10^{14}
G	1.4×10^{15}	0.066	0.138	0.237	3.1×10^{14}

gap. To do so, the experimental $n_0 = f(T)$ data points were first interpolated every 0.1 K in order to reduce the noise in the derivative calculations needed to apply the method by Hoffmann.[40] The calculated derivatives $(-kT)dn_0/dE_f$ are presented in Fig. 3 for all studied samples.

Fig. 3 shows 3 main peaks on each curve, thus confirming the presence of 3 levels in the energy range investigated (0.04–0.30 eV under E_c). Since for the well-known TD, g_1 and g_2 are, respectively, equal to 0.5 and 2, E_1 and E_2 were calculated from the peak positions after correction by $kT_{peak} \times \ln(g)$, as explained in Sec. II C. The missing E_3 values were also extracted assuming $g = 1$ and are gathered in Table II. They lie between 0.199 and 0.301 eV below E_c. The level E(0/++) of configuration X of TD2 was observed at E_c-0.25 eV,[10] E_c-0.23 eV,[14] between E_c-0.22 eV and E_c-0.24 eV,[19] and between E_c-0.23 eV and E_c-0.28 eV,[20] depending on the concentration of the defect. We therefore assign E_3 to the level E(0/++) associated with configuration X of TD2. Note that the lower E(0/++) of TD1 (E_c-0.32 eV (Ref. 14)) could not be evidenced here, as E_F does not sweep across it or merely for none of the samples. Higher T would be needed to fulfill this condition. Moreover, evidence of an ultra-shallow thermal donor (0.025–0.040 eV below E_c) was reported in TD-containing samples in Ref. 20. Similarly, this E could unfortunately not be revealed with the Hall setup used, as lower T is needed. Nevertheless, the good fit quality obtained for the different samples suggests a very low concentration for this donor, as it would otherwise shift upwards the Hall temperature curves in such a way that it would impede any satisfactory fit.

Note that the E_1 values extracted from Fig. 3 are biased since the peaks for E_1 and E_P overlap. On the contrary, the influence of P atoms is decoupled from that of TD in Fig. 2, which allowed the shallow E_1 to be determined accurately (the values extracted by both techniques remained nevertheless in excellent agreement (discrepancies were at most 8%)). Additionally, the uncertainties associated with E_1 and E_2 are higher with Hall effect spectroscopy due to the use of derivatives. For these reasons, only the values for E_3 extracted from Fig. 3 are listed in Table II, while the values of E_1 and E_2 are those extracted from Fig. 2.

The concentration of TD2 in configuration X ([X]) was estimated from the height of the peaks associated to E_3. As demonstrated in Ref. 48, the peak height indeed provides a good approximation of the defect concentration in the case of a negative U-defect. The corresponding [X] are listed in Table II. Theoretical calculations were made in order to specify the precision of the extracted [X] values, using the formalism in Ref. 47. The energy and concentration input values were varied in the ranges studied here. The extraction of the defect value using the peak height was found to be in very good agreement with the input concentration value, except when the two individual E introduced by the negative U-defect were getting closer than a couple of meV. Nevertheless, even in these conditions, the extracted values underestimate the actual values by at most 20%, and this error rapidly vanishes as the two E are split apart. As the positions of these individual E is not known in our samples, we retain this 20% error in the following as a safety rule for all samples.

B. Evolution with anneal time of the defect concentrations and energy level positions

Fig. 4 shows the values of [X] together with [TD] and the ratio of both quantities [X]/[TD]. A clear correlation appears between [X] and [TD], which further supports that both quantities are related to the same root defect. It can be seen that "old" thermal donors are significantly more abundant in configuration H. The ratio [X]/[TD] shows a saturation value at around 0.13 at prolonged anneal times, suggesting that only 1 "old" thermal donor out of 8 is eventually present in the configuration X in the studied samples.

The positions of the 3 levels introduced by annealing are plotted as a function of [TD] in Figure 5. It appears that E_1, E_2, and E_3 shift towards the conduction band as [TD] increases (i.e., as the anneal time increases). This was widely reported in the literature, particularly for E_1 and E_2 (see, for

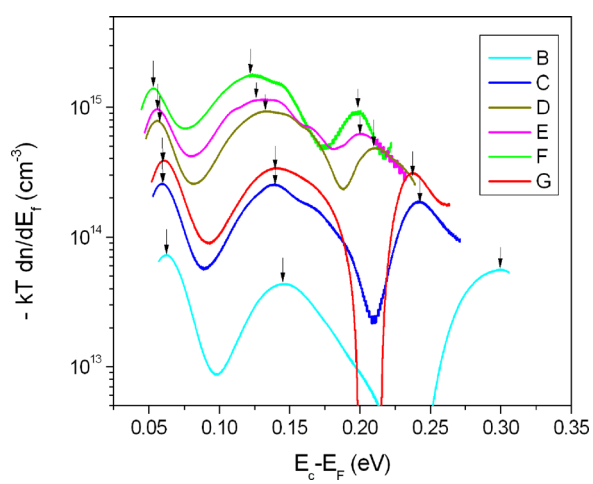

FIG. 3. $(-kT)dn/dE_F$ as a function of the Fermi energy E_c-E_F. Sample G (no 450 °C anneal, $[TD_{ini}] = 1.4 \times 10^{15}$ cm^{-3}) is also included for this spectroscopy study. The arrows indicate the approximate positions of the different E present in the samples.

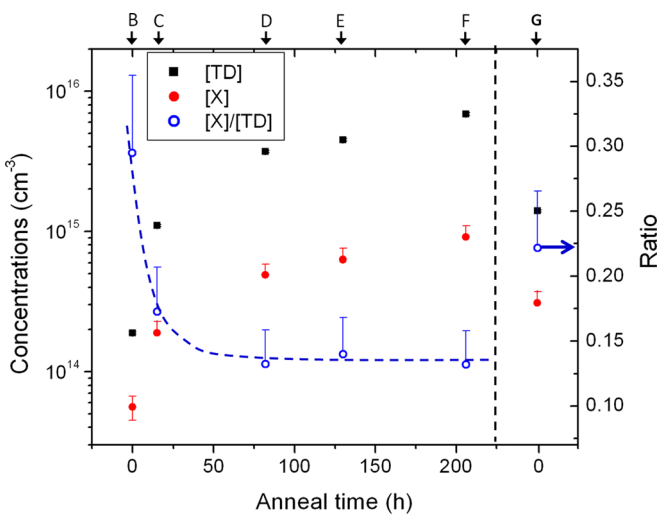

FIG. 4. Evolution with annealing time at 450 °C of the "old" thermal donor concentrations in the configuration X ([X]) and in usual configuration H ([TD]), along with the ratio of both quantities. The line is a guide for the eye.

instance, Ref. 49 or Ref. 6). This effect is shown here to be even more pronounced for E_3, moving from around 0.3 to 0.2 eV with a [TD] increase from 2×10^{14} to $6.9 \times 10^{15}\,cm^{-3}$. This is in very good qualitative agreement with Ref. 10, in which E_3 is reported to decrease from 0.27 for low TD samples down to 0.23 for higher [TD].

The results for sample G are also depicted in Fig. 5. We recall that this sample did not undergo any 450 °C anneal, and contains a large $[TD_{ini}] = 1.4 \times 10^{15}\,cm^{-3}$. Yet the values for E_1, E_2, and E_3 are in line with the results obtained for the 450 °C annealed samples. We conclude that the T of generation of "old" thermal donors does not influence (within experimental errors) the positions of the different E. This additionally suggests that the stoichiometry of TD in both possible configurations (H and X) are comparable in as-grown samples and in 450 °C annealed samples, provided that they have similar [TD].

C. Identification of the carrier lifetime-limiting level

The position of the main recombination-active level was extracted on sample F, containing the highest [TD]. This sample was selected since τ_{eff} in the 21–185 °C range did not exceed 150 μs and could thus be measured under one single measurement mode (here quasi-steady state), suppressing possible unwanted uncertainties arising from a mode change. It had also the advantage of featuring $\tau_{eff} \ll \tau_{surf}$ and $\tau_{eff} \ll \tau_{int}$ (over 5 ms at room T in this sample). As a consequence, any T variations in τ_{surf} and τ_{int} could be neglected in the extraction of τ_{SRH} using Eq. (5).

Due to photogeneration-induced E_F shifts, bistable TD could switch from the H and X configurations (and vice versa) under illumination.[14] It was thus necessary to check beforehand whether the flashes used for the τ_{eff} measurements lead to any change in the respective X and H populations. To this end, we performed temperature Hall effect measurements in the dark on an extra TD containing sample

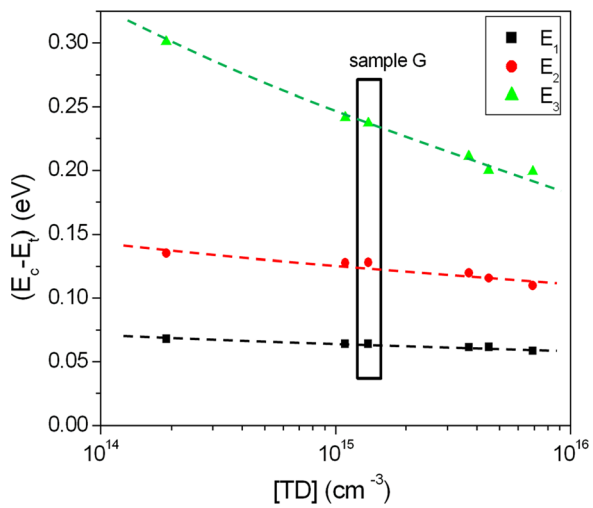

FIG. 5. Positions of the energy levels introduced during 450 °C annealing. The measurements for sample G (no 450 °C anneal, $[TD_{ini}] = 1.4 \times 10^{15}\,cm^{-3}$) are also shown. Dashed lines are guides for the eye. As throughout the text, [TD] corresponds to the concentration of the defect in configuration H.

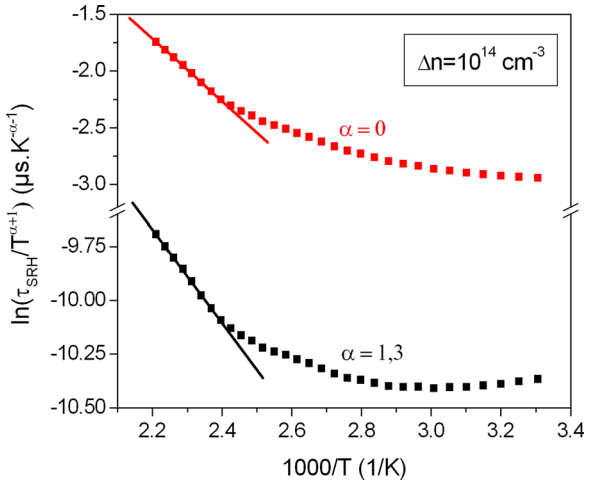

FIG. 6. Data used for the extraction of the energy level related to the lifetime-limiting defect for sample F. Lines are fits using Eq. (4).

([TD] around $2 \times 10^{15}\,cm^{-3}$) before and directly after applying a large amount of flashes to the sample (around 20). The flashes used were identical to those used for the τ_{eff} measurements. Flashing was performed both at room T as well as 185 °C, the latter being the maximum temperature used here for τ_{eff} measurements. The sample used was passivated, in order to ensure that the injection conditions were the same as during τ_{eff} measurements. The passivation layer was scratched away when creating the InGa contacts, thus providing ohmic contacts necessary to the Hall measurements. This preliminary study led to no changes in the Hall curves within measurement uncertainties, demonstrating that if X and H populations were modified, this effect was largely negligible. Therefore, the τ_{eff} measurements from this section and the following are representative of the TD populations as listed in Table II.

Fig. 6 shows the data points calculated from Eq. (4) from the $\tau_{eff} = f(T)$ curves for two different α coefficients: α was first arbitrarily set to 0, and subsequently to 1.3, as estimated on a sample with $[TD] = 2 \times 10^{15}\,cm^{-3}$ in Ref. 24 from low-T τ_{eff} measurements according to the method given in Ref. 41. The τ_{SRH} values were calculated using Eq. (5) from the experimental τ_{eff} data at $\Delta n = 10^{14}\,cm^{-3}$ (low injection condition for all samples). The depicted lines are the fits from which E_t associated to the lifetime-limiting defect were extracted.

Depending on the α coefficient used, and under the assumption that ΔE_t is T-independent, ΔE_t was found equal to 0.19 ± 0.01 ($\alpha = 1.3$) or 0.24 ± 0.01 eV ($\alpha = 0$). Note that the same work was performed on sample E (not shown here) and led to similar E_t values. Additional information on the defect localization was brought as a result of the fitting procedure of room-T τ_{eff} curves (see Sec. III D), which turned out to be only possible for a defect in the upper-band gap. Therefore, the value obtained with $\alpha = 1.3$ is consistent with E_3 of sample F, located at E_c-0.199 eV. The latter match thus suggests that TD2 in configuration X are responsible for the lifetime limitation in TD containing samples. This result was predicted in Ref. 19 and is supported by our findings. However, it should be mentioned that we cannot rule out the

presence of another defect which would introduce an E in the same energy range and would be present in too low concentrations to be detected by Hall measurements. Despite these uncertainties, further discussed in Sec. III D in the light of the capture cross section results, assuming that TD2 in configuration X allows us to derive a complete SRH parameterization for recombination through TD, given at the end of the paper. In the following, it will therefore be taken as a working hypothesis that the carrier lifetime-limiting level E_t is E_3 for all samples and thus that $N_t = [X]$.

As pointed out in Ref. 45, the simplified SRH model used to derive Eq. (4) is accurate provided that N_t be at least an order of magnitude smaller than a value N_{crit}, which is mainly a function of n_0, Δn, σ_p, and σ_n. Although deep centers such as metallic or dopant-metallic impurities generally fulfill this condition, it was not clear here since [X] is relatively large. After verification, we found however that this condition holds true for the sample F used here, and so whatever Δn and T > room T (assuming the same variations with T for σ_p and σ_n). For instance, we found that in the worst case (room T), $N_{crit} = 9.5 \times 10^{15}\,cm^{-3}$, which is greater than $10 \times [X] = 10 \times 9.1 \times 10^{14}\,cm^{-3}$. The use of Eq. (4) also requires that $n_1/n_0 \gg 1$,[41] where n_1 is the value of n_0 if E_F is set equal to E_t. This is verified for sample F since in the T range used for the slope extraction (T > 410 K), $n_1 > 1.9 \times 10^{17}\,cm^{-3}$, which is over one decade larger than n_0. The use of Eq. (4) is therefore justified and supports the validity of the value extracted for E_t. Note that the existence of another linear portion at lower T in the Arrhenius plot of Fig. 6 could suggest the presence of a secondary (i.e., not dominant[41]) recombination level. However, due the poor E-resolution of TDLS[41] combined to the unsatisfied conditions for the validity of the simplified SRH model at lower T, no attempt was made to further characterize this potential secondary E.

D. Room temperature carrier lifetime measurements and SRH parameterizations

Fig. 7 presents the experimental τ_{eff} data along with the fits using Eq. (5), under the hypothesis that the same E_3 limits τ_{SRH} in all samples. Note that τ_{eff} was significantly improved after TDA (sample A), up to around 8 ms (not shown here). This is likely to be explained by a combination of effects, such as the dissolution of grown-in defects,[31,32] an internal gettering of fast-diffusing impurities on grown-in O precipitates,[50] and the dissolution of TD. Notice also that Sample G was not included since a τ_{eff} mapping using MicroWave-detected PhotoConductance Decay (μW-PCD) revealed a black-core pattern which remained after high T steps (>800 °C), suggesting the presence of large concentrations of recombination active defects other than TD (likely to involve O-precipitates).

Fig. 7 shows that for the low [TD] range (up to sample C, $[TD] = 1.1 \times 10^{15}\,cm^{-3}$), TD are very well tolerated since τ_{eff} remains above 1 ms. On the contrary, larger [TD] led to much lower τ_{eff}, resulting in material properties significantly out of specifications for state of the art HET solar cells. For instance, τ_{eff} of sample F ($[TD] = 6.9 \times 10^{15}\,cm^{-3}$) is

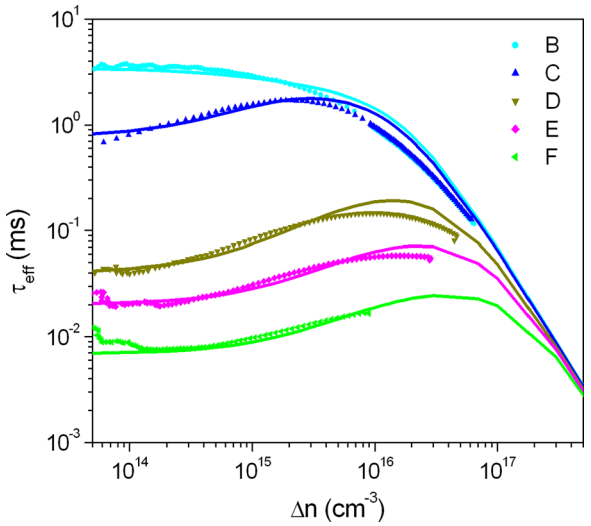

FIG. 7. Effective carrier lifetime data measured for the various samples (data points) and related best fits (lines) obtained with the SRH recombination parameters of the defect X as listed in Table II.

reduced to a few μs at low Δn! In order to model τ_{SRH}, the experimentally determined [X] and E_3 were used as N_t and E_t input values. Then, the capture cross sections σ_n and σ_p were varied in order to fit the entire experimental curves. It was found that a unique couple of σ_n-σ_p was possible, except for sample B for which σ_n was poorly influencing the results and could thus not be determined. The uncertainties were estimated from the loss in fitting quality to be around 5% for σ_p and 10% for σ_n. We also checked for all samples that $N_{crit} > 10 \times [X]$ at room T, in order to safely apply the simplified SRH statistics. This was verified for all samples whatever Δn, except for samples C and D for which it was only valid above $\Delta n = 5 \times 10^{14}\,cm^{-3}$, i.e., for most of the Δn range studied here. Note that the fits obtained at high Δn slightly overestimate the actual τ_{eff} values. Such deviation could either be due to the involvement of a second recombination-active level, but it may as well just be the result of variations in τ_{surf} from the parameterization used in this work (see Sec. II D). Therefore, no attempt to further characterize this hypothetic second level was made. It is also of interest to mention here that carrier trapping is observed at low Δn on samples with the highest [TD], as already observed in Ref. 21.

The τ_{eff} values as extracted at $\Delta n = 5 \times 10^{14}\,cm^{-3}$ are plotted as a function of [TD] in Figure 8. The data by Hu *et al.*[21] are also plotted. The authors used carrier density imaging (CDI) to investigate in detail the effect of TD on the local τ_{eff} on a single as-grown vertical cut taken from an industrial Cz ingot. Although Δn in their case could not be accurately determined, a good agreement can be observed between both sets of data. In particular, the sudden τ_{eff} decrease above $[TD] = 10^{15}\,cm^{-3}$ is observed in both studies, while τ_{eff} for low [TD] is mainly determined by τ_{surf} (different for both studies). This inter-study correlation strongly supports the absence of large unintentional contamination during the 450 °C anneals we performed to adjust [TD] (no anneals were done in the study by Hu *et al.*, so that no contamination could occur).

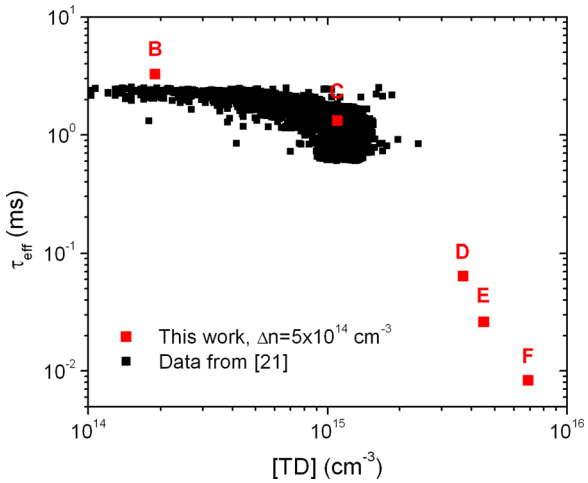

FIG. 8. Effective carrier lifetime as a function of [TD]. The data of this work were extracted at $\Delta n = 5 \times 10^{14}\,cm^{-3}$. The data from Ref. 21 were measured using CDI. Discrepancies at low Δn are related to differences between the two studies in passivation efficiency of the dielectric layers.

σ_n and σ_p are plotted together with their ratio (k) as a function of [X] in Fig. 9. As expected from the order-of-magnitude decrease in τ_{eff} with increasing [TD], Fig. 9 shows that both σ_n and σ_p rapidly increase with [TD]. Under the assumption that TD2 in configuration X is the lifetime-limiting defect, this is evidence of an increased recombination activity with 450 °C annealing time. This increase may appear misleading since in the usual picture, capture cross sections are not expected to vary with the defect concentration. However, it was shown that E_3 is due to TD2 in configuration X, and that it is [X]-dependent (Ref. 10, this study). This is not expected either in the usual picture where the E is independent of the defect concentration. Thus, we believe that our observations are compatible with evolving capture cross sections with annealing time. This increase could highlight a gradual change in defect stoichiometry and electronic configuration, as supported by the shift of E_3 (Fig. 5) with annealing time at 450 °C. Alternatively, TD2 in configuration X could also be in fact a set of very closely related individual defects with evolving populations and individual recombination parameters. This remains however to be further investigated in-depth.

E. Simulations results

Fig. 10 presents the simulation results regarding the conversion efficiency η for the different cell architectures modeled, based on the SRH and doping parameters extracted from this work. The SRH parametrization is performed from $5 \times 10^{13}\,cm^{-3}$ to $5 \times 10^{16}\,cm^{-3}$ excess minority carrier density, which covers more than the range swept during a standard current-voltage measurement of an operating cell under AM1.5 illumination (typically from 10^{14} to $10^{16}\,cm^{-3}$). The parametrization therefore remains valid whatever the voltage from short-circuit to open-circuit conditions. It is tacitly assumed here that unintentional TD_{ini} (of interest for wafer/cell manufacturers) have similar recombination activities as intentionally generated TD at 450 °C. This assumption is supported by the very good consistency of the results of Fig. 5 for annealed and non-annealed samples. Regarding Fig. 10, η appears to be strongly reduced when [TD] is increased, as expected from the τ_{eff} measurements. This is particularly true for rear emitter cells, which show a larger sensitivity of the η with τ_{eff}. For instance, η is reduced to less than 5% for $[TD] = 6.9 \times 10^{15}\,cm^{-3}$ compared to $\eta \sim 15\%$ for standard emitter cells. The η reduction was found to be primarily related to short circuit current drops, up to 75% at the highest [TD]. The current drops were particularly large for rear emitter structures, owing to a stronger sensitivity to τ_{bulk} due to a longer average distance for photogenerated holes to reach the emitter. Significant open circuit voltage reductions were also observed, with a similar amplitude for rear/front emitters and standard/advanced structures (15% drop at the highest [TD]). The fill factor showed little variations.

As an inset in Fig. 10, a zoom is presented for $[TD] < 1.5 \times 10^{15}\,cm^{-3}$, which is the typical [$TD_{ini}$] range in commercial Cz wafers. This inset shows that regardless of the architecture, there is a 1%–2% abs. loss in η between a

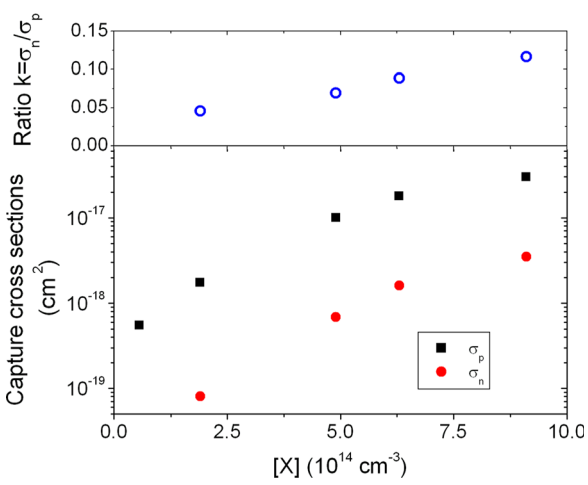

FIG. 9. σ_n and σ_p values extracted from the fitting of room-temperature lifetime curves for the different samples (bottom), along with the ratio of both quantities (top).

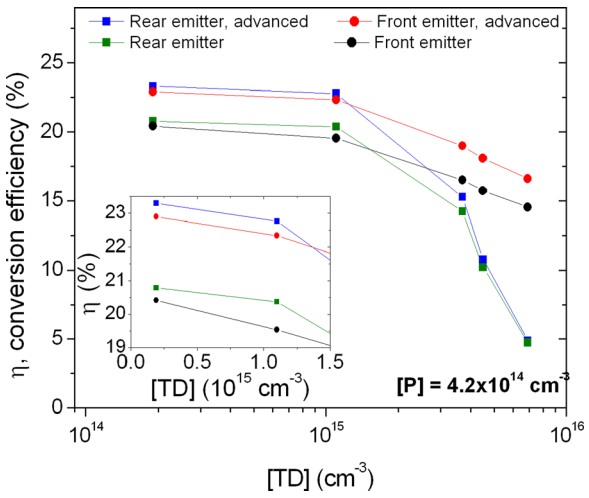

FIG. 10. Simulation results showing the variations of the conversion efficiency (η) with [TD]. The inset shows a zoom in the [TD] range met in commercial Cz ingots. Lines are a guide for the eyes.

wafer without TD and a wafer with [TD] = $1.5 \times 10^{15}\,cm^{-3}$. This is consistent with the experimental results obtained by Jay *et al.*[26] The authors studied rear emitter HET cells made on substrates only doped with TD. They evidenced a net reduction from $\eta = 20.2\%$ at low [TD] to around $\eta = 18.2\%$ at [TD] = $1.75 \times 10^{15}\,cm^{-3}$.

This result outlines the fact that [TD] (or more exactly [X]) should therefore be kept to a minimum, for instance, by lowering [O_i] (although the dependence of [X] in as-received wafers upon [O_i] remains to be studied) or by increasing the crystal cooling speed. This will be even more challenging for future larger ingots, whose thermal mass will favor slower cooling rates and larger generation of thermal defects. Alternatively a killing of TD using TDA can also be used, when possible. In addition to annihilating virtually all TD (shown in Sec. III A), such TDA treatments also have the potential to dissolve grown-in defects involving vacancies[31,32] or promote internal gettering of fast diffusing impurities on O-precipitates.[49]

IV. CONCLUSIONS

The aim of this work was to specify the recombination activity associated with TD in commercial Cz Si and to assess the efficiency reduction expected from the presence of TD in heterojunction solar cells. To this end, wafers with a wide range of defect concentrations were prepared as a starting point, and a series of advanced characterization techniques and simulations were used. The main conclusions of this work can be summarized as follows:

- As already observed in the literature, we evidenced that three donor levels are introduced during the course of TD formation at 450 °C. The two shallowest are related to the historically studied configuration of TD, while the deepest level corresponds to another configuration (X) of the bistable TD2 family.
- TD deliberately formed at 450 °C introduce the same levels as those generated unintentionally during ingot cool down. This brings new knowledge about TD generation as it suggests that regardless of the formation temperature, the generated donors have similar stoichiometry for a given [TD], and probably similar recombination activities (although this should be further validated).
- To the best of our knowledge, we report for the first time a tentative identification of the carrier lifetime-limiting level in TD-containing Si. Our results suggest that TD2 in configuration X limits the lifetime. Some uncommon properties of the defect were however pointed out and will have to be further investigated to validate this identification. The defect concentration [X] was measured in the range of 10^{13}–$10^{15}\,cm^{-3}$, noticeably lower than the concentration of TD in standard configuration H. In very good agreement with the literature, the location of the defect energy level is reported to lie between 0.199 and 0.301 eV below the bottom of the conduction band, depending on 450 °C annealing time. This results points out the necessity that future researches on trace yet recombination-active defects in high lifetime Si be carried out on samples with low [X].
- It was found that τ_{eff} was very strongly reduced for extended TD generation (down to a few μs), resulting in material properties way out-of-specifications for state-of-the-art HET cell architectures. On the contrary, low [TD] appeared to be very well tolerated up to around $5–10 \times 10^{14}\,cm^{-3}$, enabling multi-millisecond carrier lifetimes. Note that this holds true for homogeneously distributed TD. This range may be somewhat lowered if TD are heterogeneously distributed (common in practice), due to associated radial ρ and τ non-uniform distributions, which can be detrimental to the cell efficiency.
- We defined a first SRH parameterization for TD2 in configuration X, under the working hypothesis that the latter defect limits the lifetime. Using the established SRH parameterization, simulations were run for advanced and standard rear and front emitter HET solar cells. It was found that [TD] larger than $1–1.5 \times 10^{15}\,cm^{-3}$ (fortunately unusual in current crystals) led to very low conversion efficiency, down to 5% in the worst case. In good agreement with the literature, it was underlined that for [TD] in the upper range of what is met in today's commercial ingots (i.e., up to $1–1.5 \times 10^{15}\,cm^{-3}$), a large η reduction of around 1%–2% abs. is to be dealt with. Our results urge premium wafer providers and high efficiency HET manufacturers to keep [TD] as low as possible, in order to reach higher τ_{eff} and a tighter radial ρ uniformity.

ACKNOWLEDGMENTS

This work was carried out in the frame of the project HERCULES. The project HERCULES has received funding from the European Union's Seventh Programme for research, technological development and demonstration under Grant Agreement No. 608498. J. Veirman thanks V. V. Voronkov for fruitful discussions on charge states of thermal donors.

APPENDIX: IMPLEMENT TD RECOMBINATION PROPERTIES IN DEVICE SIMULATION

We provide here simple expressions that will allow the reader to easily implement the published data into device simulation, in order to estimate the effect of TD on device performance. By further analyzing the data of graphs 4, 5, and 9, empirical relationships were derived allowing one to compute from a given measured [TD] the input data to be fed into SRH recombination calculations,[45,46] namely, [X], E_3, σ_n, and σ_p. Note that the provided expressions were established on samples having $1.9 \times 10^{14}\,cm^{-3} < [TD] < 6.9 \times 10^{15}\,cm^{-3}$ and care should be taken when used beyond this range. Parameterizations may also be somehow less accurate for [TD] between $1.9 \times 10^{14}\,cm^{-3}$ and $1.1 \times 10^{15}\,cm^{-3}$ due to the lack of samples in this range.

It was found that [X] (cm^{-3}) could be calculated from [TD] (cm^{-3}) using

$$[X] = 0.1268 \times [TD] + 3.956 \times 10^{13}. \quad \text{(A1)}$$

E_3 can be accurately described as a function of [TD] (cm^{-3}) using

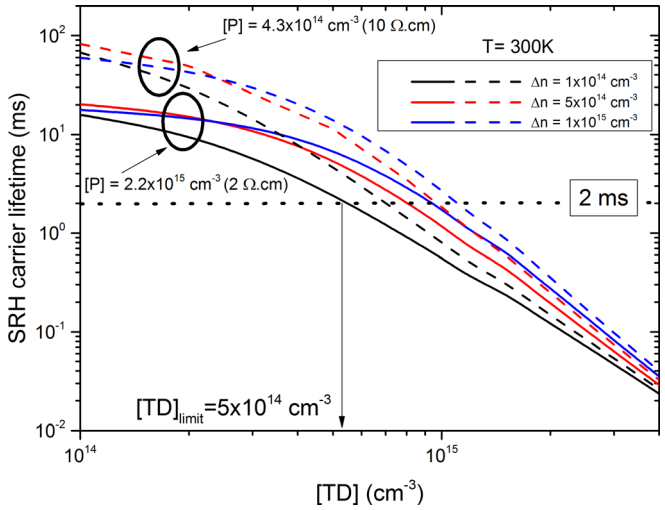

FIG. 11. Calculated variations in SRH lifetime as a function of measured [TD] using Eqs. (A1)–(A4) to calculate the input data to be fed into the SRH calculations ([X], E_3, σ_n, and σ_p).

$$E_3(\mathrm{eV}) = 15.46 \times [TD]^{-0.12}. \tag{A2}$$

Finally, the variations with [X] (cm^{-3}) of σ_n and σ_p can be empirically reproduced using

$$\sigma_n(\mathrm{cm}^2) = 3.16 \times 10^{-54} \times [X]^{2.41}, \tag{A3}$$

$$\sigma_p(\mathrm{cm}^2) = 4.01 \times 10^{-40} \times [X]^{1.53}. \tag{A4}$$

Using the set of expressions (A1)–(A4), we computed the SRH lifetime variations as a function of [TD] in Fig. 11 for 3 different Δn relevant to HET operation. In good agreement with our conclusions, $[TD] = 5 \times 10^{14}$–$10^{15}\,\mathrm{cm}^{-3}$ constitutes an upper limit values for $\tau_{SRH} > 2\,\mathrm{ms}$. In practice, such values are only likely to be met in the slow-cooling top ingot fraction. In nowadays standard ingots dedicated to HET cells production, a typical [P] for this fraction is between 3 and $5 \times 10^{14}\,\mathrm{cm}^{-3}$, and therefore the maximum acceptable [TD] value can be refined from Fig. 11 to be around $7 \times 10^{14}\,\mathrm{cm}^{-3}$. This yields a lower acceptable ρ value at the wafer center of 2.6 Ω cm. Including a typical τ_{surf} component of $2\,\mathrm{cm\ s}^{-1}$ in the calculation, while having a 2 ms effective lifetime target, yields a slightly higher value of 3 Ω cm. These values can be used as a rule of thumb to readily estimate the bulk quality of such top-ingot wafers.

[1]C. S. Fuller and R. A. Logan, J. Appl. Phys. **28**, 1427–1436 (1957).
[2]F. Shimura, *Oxygen in Silicon* (Academic, New York, 1994), Chap. 7.
[3]H. J. Stein, S. K. Hahn, and S. C. Shatas, J. Appl. Phys. **59**, 3495 (1986).
[4]*Properties of Crystalline Silicon*, edited by R. Hull (INSPEC, The Institution of Electrical Engineers, London, 1999), p. 270.
[5]W. Wijaranakula, Appl. Phys. Lett. **59**, 1608–1610 (1991).
[6]D. Wruck and P. Gaworzewski, Phys. Status Solidi A **56**, 557 (1979).
[7]W. Gotz, G. Pensl, and W. Zulehner, Phys. Rev. B **46**, 4312–4315 (1992).
[8]T. Hallberg and J. L. Lindström, J. Appl. Phys. **79**, 7570 (1996).
[9]M. Bruzzi, D. Menichelli, and M. Scaringella, J. Appl. Phys. **99**, 093706 (2006).
[10]H. J. Hoffmann, Appl. Phys. A **33**, 47–50 (1984).
[11]F. Jay, J. Veirman, M. Tomassini, R. Peyronnet-Dremière, A. Danel, C. Denis, J. Stadler, J.-C. Helleboid, D. Muñoz, S. Dubois, and A. Jouini, in Proceedings of the 29th European Photovoltaic Solar Energy Conference and Exhibition, The Netherlands, Amsterdam, 2014.
[12]V. D. Tkachev, L. F. Makarenko, V. P. Markevich, and L. I. Murin, Sov. Phys. Semicond. **18**, 324 (1984).
[13]L. F. Makarenko, V. I. Markevich, and L. I. Murin, Sov. Phys. Semicond. **19**, 1192–1195 (1985).
[14]Y. I. Latushko, L. F. Makarenko, V. P. Markevich, and L. I. Murin, Phys. Status Solidi A **93**, K181 (1986).
[15]P. Wagner and J. Hage, Appl. Phys. A **49**, 123–138 (1989).
[16]A. Chantre, Appl. Phys. Lett. **50**, 1500 (1987).
[17]P. W. Anderson, Phys. Rev. Lett. **34**, 953 (1975).
[18]H. J. Hoffmann, Phys. Rev. Lett. **45**, 1733–1737 (1980).
[19]F. Dreckschmidt, V. Osinniy, M. Herms, and J. Neusel, in Proceedings of the 28th European Photovoltaic Solar Energy Conference and Exhibition, Paris, 2013.
[20]H. Nakayama, J. Katsura, T. Nishino, and Y. Hamakawa, Jpn. J. Appl. Phys., **19**, 547–550 (1980).
[21]Y. Hu, H. Schøn, E. J. Øvrelid, Ø. Nielsen, and L. Arnberg, AIP Adv. **2**, 032169 (2012).
[22]D. L. Bätzner, L. Andreerra, W. Frammelsberger, R. Kramer, D. Lachenal, B. Legradic, J. Meixenberger, P. Papet, F. Rigoletti, B. Strahm, and G. Wahli, in Proceedings of the 30th European Photovoltaic Solar Energy Conference and Exhibition, Hambourg, 2015.
[23]F. Jay, J. Veirman, N. Najid, D. Muñoz, S. Dubois, and A. Jouini, Energy Procedia **55**, 533–538 (2014).
[24]N. Najid, J. Veirman, J. Stendera, F. Jay, and R. Monna, nPV workshop, Chambéry, 2013.
[25]S. Binetti, M. Acciarri, A. Brianza, C. Savigni, and S. Pizzini, Mater. Sci. Technol. **11**, 665–669 (1995).
[26]F. Jay *et al.*, in Proceedings of the 30th European Photovoltaic Solar Energy Conference and Exhibition, Hambourg, 2015.
[27]J. Veirman, S. Dubois, N. Enjalbert, J. P. Garandet, D. R. Heslinga, and M. Lemiti, Solid State Electron. **54**, 671–674 (2010).
[28]M. Claybourn and R. C. Newman, Appl. Phys. Lett. **52**, 2139–2141 (1988).
[29]S. De Wolf, A. Descoeudres, Z. C. Holman, and C. Ballif, Green **2**, 7–24 (2012).
[30]D. B. M. Klaassen, Solid-State Electron. **35**, 953 (1992); **35**, 961 (1992).
[31]P. Zheng, F. E. Rougieux, N. E. Grant, and D. Macdonald, IEEE J. Photovoltaics **5**(1), 183–188 (2015).
[32]F. E. Rougieux, N. E. Grant, and D. Macdonald, Phys. Status Solidi RRL **7**, 616–618 (2013).
[33]J. Veirman, S. Dubois, N. Enjalbert, and M. Lemiti, Energy Procedia **8**, 41–46 (2011).
[34]M. Cascant, J. Veirman, M. Tomassini, R. Peyronnet, N. Enjalbert, J. Stadler, E. Fayard, S. Dubois, J.-C. Helleboid, L. Bonis, P. Bonnard, X. Brun, E. Girot, and J.-Y. Poriel, in Proceedings of the 8th SNEC conference, Shanghai, 2014.
[35]J. Veirman, S. Dubois, N. Enjalbert, J. P. Garandet, and M. Lemiti, Phys. Status Solidi C **8**, 729 (2011).
[36]E. Ohta and M. Sakata, Jpn. J. Appl. Phys., Part I **17**, 1795–1804 (1978).
[37]J. Veirman, Ph.D. thesis, INSA de Lyon, 2011.
[38]R. G. Aggarwal and A. K. Ramdas, Phys. Rev. **140**, A1246 (1965).
[39]D. C. Look, Phys. Rev. B **24**, 5852–5862 (1981).
[40]H. J. Hoffmann, Appl. Phys. **19**, 307–312 (1979).
[41]S. Rein, *Lifetime Spectroscopy*, Springer Series in Materials Science (Springer-Verlag, Berlin Heidelberg, 2005), Vol. 85, p. 492.
[42]R. Sinton, A. Cuevas, and M. Stuckings, in *Proceedings of the 25th IEEE Photovoltaic Specialists Conference Record* (1996), pp. 457–460.
[43]A. Richter, S. W. Glunz, F. Werner, J. Schmidt, and A. Cuevas, Phys. Rev. B **86**, 165202 (2012).
[44]E. Yablonovitch and T. Gmitter, Appl. Phys. Lett. **49**, 587 (1986).
[45]D. Macdonald, Ph.D. thesis manuscript, The Australian National University, 2001.
[46]D. Macdonald and A. Cuevas, Phys. Rev. B **67**, 075203 (2003).
[47]R. Varache, N. Nguyen, and D. Munoz, Energy Procedia **55**, 149–154 (2014).
[48]H. J. Hoffmann, Appl. Phys. A **27**, 39–47 (1982).
[49]C. D. Lamp and B. D. Jones, Appl. Phys. Lett. **58**, 2114 (1991).
[50]J. D. Murphy, R. E. McGuire, K. Bothe, V. V. Voronkov, and R. J. Falster, J. Appl. Phys. **116**, 053514 (2014).